Case Studies in Thermal Engineering 45 (2023) 102897

Contents lists available at ScienceDirect

Case Studies in Thermal Engineering

journal homepage: www.elsevier.com/locate/csite

Mathematical model for numerical simulations of thermal energy of nano-fluid in a complex peristaltic transport within a curved passage:Pharmacological and engineering biomedical application

Nahid Fatima [a], Khulud Alayyash [b], Wafa F. Alfwzan [c], Nouman Ijaz [d,*], Arshad Riaz [e], Najma Saleem [f], ElSayed M. Tag El-Din [g]

[a] Department of Mathematics and Sciences, Prince Sultan University, Riyadh, 11586, Saudi Arabia
[b] University School of Mathematics, Senghennydd Rd, Cardiff, CF24 4AG, United Kingdom
[c] Department of Mathematical Sciences, College of Science, Princess Nourah bint Abdulrahman University, P.O. Box 84428, Riyadh, 11671, Saudi Arabia
[d] Department of Mathematics and Statistics, Punjab Group of Colleges, G.T. Road Jada, Jhelum, 49600, Pakistan
[e] Department of Mathematics, Division of Science and Technology, University of Education, Lahore, 54770, Pakistan
[f] Department of Mathematics and Natural Sciences, Prince Mohammad Bin Fahd University, Khobar, 31952, Saudi Arabia
[g] Center of Research, Faculty of Engineering, Future University in Egypt, New Cairo, 11835, Egypt

ARTICLE INFO

Keywords:
Complex travelling wave
Peristaltic transport
Nano-fluid
Electro-osmosis
Magnetohydrodynamics
Ohmic heating dissipation
Curved channel

ABSTRACT

The proposed scientific model is based on peristaltic movement of nanofluid within a curved channel of an electrically conducting material. To obtain a numerical solution for the electric potential function, the Debye-Hückel and Lubrication theory approximations are used. Stream function, electroosmotic, axial velocity, and curvature are all estimated using low zeta potentials. The behaviour of electroosmotic flow governs two dimensionless parameters: the Debye-Hückel parameter and the Helmholtz-Smoluchowski velocity. It is also investigated how curvature influences blood flow caused by electroosmosis. It was also investigated how the curvature parameter affects the nano-fluid flow induced by electroosmosis. Nano-biofluid evaluation with varied particle shapes such as cylinder, platelet, brick, and blade flowing in complex travelling wave. It can be stated that the velocity component of nanofluid is decreasing due to magnetic force, particle size, and wall compliance. It is also stated that nanoparticles considerably improve the thermal conductivity of the fluid.

Nomenclature

$\widetilde{U}, \widetilde{V}$	Velocity components
$\overline{X}$	Axial direction
$\overline{R}$	Radial direction
$\widetilde{R}^{*}$	Curved channel
b_1, b_2	Wave amplitudes
C	Wave velocity

* Corresponding author.
E-mail address: noumanijaz666@gmail.com (N. Ijaz).

https://doi.org/10.1016/j.csite.2023.102897
Received 8 January 2023; Received in revised form 23 February 2023; Accepted 11 March 2023
Available online 14 March 2023
2214-157X/© 2023 The Authors. Published by Elsevier Ltd. This is an open access article under the CC BY license (http://creativecommons.org/licenses/by/4.0/).

A	Semi width
R_e	Reynold number
B_0	Magnetic field
P	Pressure in fixed frame
M	Hartmann number
m	Electro-osmostic parameter
$\widetilde{T}_0, \widetilde{T}_1$	Constant temperature
E_1	Tension wall
E_2	Mass wall
E_3	Damping nature
Gr	Grashoff Number
μ_s	Viscosity of the fluid
σ	Electric conductivity of the fluid
λ	Wavelength
ρ_{nf}	Fluid density
k_{nf}	Thermal conductivity
α_{nf}	Thermal diffusibility
$C_{p_{nf}}$	Specific heat
β_{nf}	Thermal expansion coefficient
χ	Concentration of nanoparticles
f	Shape factor
C_k^{Shape}	Thermal conductivity due to shape
$C_k^{Surface}$	Resistance due to surface
ψ	Sphericity
R_k	Kapitza Resistance
l_k	Kapitza length
A_1, A_2	Viscosity enhancement coefficients
Subscript	
f	Base fluid
s	Solid nanoparticles
nf	Nanofluid

1. Introduction

In the current century, the technology of nanofluid is emerged as the latest enhanced technique of heat transfer. The nanofluids are generated with the suspensions of nanomaterials and base fluids. The nanomaterials are often utilized for the formulation of nano-sheets, nanorods, nanowires, nanotubes, nanofibers, and nanoparticles. The nanofluids have enhanced thermophysical properties like viscosity, thermal diffusivity, and thermal conductivity. Due to this feature nanofluids provide better performance as compared with base fluids such as oil and water. The technology of nanofluid can assist to evolve better lubricants and oils for practical applications. The nanofluid flow applications can be found in many areas for instance, spray-coating, reacting surfaces and catalysts, boiling phenomena, drug delivery, surgery, cancer therapy, heat exchanger design, microelectronics, microchannels, power generation and micromanufacturing processes. These applications have attracted the researchers to work in the field of nanofluids in various directions. Feng and Kleinstreuer [1] have provided the detailed review and applications of nanofluid motion between the disks. Wong and Leon [2] have presented the current and future applications of nanofluids in various engineering and industrial purposes. Menni et al. [3] have collected detailed numerical, experimental, and theoretical studies of nanofluids and their applications in modern lifestyle. Ali et al. [4] have given a detailed review on nano-liquids in the direction of thermophysical properties, stability, and fabrication. Kleinstreuer and Xu [5] have provided the fundamental knowledge and applications of nano-liquids related to cooling and lubrication. Kasaeian et al. [6] have presented the detailed review on the latest developments of heat exchange and nanofluid stream in void medium. Tassaddiq et al. [7] have used homotopy method to discuss the nanofluid propulsion over a rotating disk and noted that the submission of nanoparticles in primary fluids has enhanced the heat and mass exchange rates. Mahdavi et al. [8] have made the tabulated investigation on the Poiseuille flow of nano-sized particle presence inside the flow in a channel and concluded that the Brownian motion plays a powerful part in migration of nanoparticles. Mondal and Pal [9] have found the bioconvection nanofluid along a stretching sheet using Mathematica software and said that this study has applications in bio-nano-coolant systems and energy conversion devices. Laila and Dil [10] have discussed the propulsion of nano-liquid in a diverging/converging channel using the perturbation method and concluded that the temperature enhances faster along the nanoparticle concentration.

Nowadays the use of MHD in the flow characteristics of fluid has become core objective to the current investigations. MHD is the study related to the electrically induced fluid flows affected by an imposed magnetic force. The part of MHD is substantial in the field of

fluids system and keeps several engineering and industry-based applications. Few applications include, plastic extrusion, MHD accelerators, fiber production, crystal growth, polymer technology, metalworking, boundary layer control, hydro-magnetic motors. In metallurgy, electro-MHD can be helpful in the producing the quality of the final product. MHD also have many biomedical applications such as, in cancer therapy, biomedical sensors, MHD micropump, tumor treatment, magnetic resonance imaging (MRI) and cellular separation. These motivations and applications have created the interest in many researchers to study the MHD effects in diverse fluid flow geometries. For instance, Alghamdi et al. [11] have provided the mathematical model on the nanofluid motion in the rectangular permeable channel using homotopy method and concluded that MHD has the salient features in blood flow. Mehmood et al. [12] have considered the MHD nano-particles flow past a rotating disk using bvp4c technique, and provided that the stronger magnetic field deteriorating the velocity profile. Elgazery [13] discussed the unsteady 3D motion of nano-liquid over the stretching surface using shooting method and observed that maximum temperature is acquired by adding silver nanoparticles in base fluid. Loganathan et al. [14] have used homotopy method to investigate the nanofluid motion over a heated Riga plate and noted that the higher temperature is found for nanofluid case as compared with viscous fluid case. Hayat and Nadeem [15] have discussed MHD flow of nano-liquids over a stretched plane with stagnation point using optimal-HAM. Ahmad et al. [16] have produced approximate solutions for the magnetized 3D motion of Ferro and given that exponent parameter of temperature enhances the rate of heat transfer. Few more studies can be seen with respect to MHD and nanofluid flow in diverse situations in references [17–23] and the references therein.

Radially regular muscles recreation and reduction occurs in muscular hose, which generates the wave structures in a sequential manner. This process is known as peristaltic mechanism. In the living bodies, this mechanism arises with smooth muscles contraction pushes the biofluid in the digestive system. The similar kind of mechanism is used by earthworms to drive their locomotion. There are many other situations are observed in physiology such as finger pumps, roller pumps, chyme movement, food transport and urine transport. The transport phenomenon of peristalsis along with MHD and nanomaterials has received much interest due to their emerging applications. Abbas et al. [24] have discussed the MHD motion of blood-nano-liquid in a non-uniform peristaltic channel employing the analytic method. Tanveer et al. [25] have presented a theoretical investigation on the peristaltic study of MHD nanoparticles in Carreau fluid across a bended structure. Tanveer et al. [26] have studied the MHD peristaltic scheme of Jeffrey model-based nano-liquid in a curved geometry using the well-known numerical method. Noreen et al. [27] have gathered the approximate solutions by using technique of Shooting scheme for the MHD peristaltic nanofluid flow in a bended shape conduit. Tanveer et al. [28] have modeled the peristaltic MHD Powell-Eyring nano-liquid flow in a curved geometry. Ahmed and Rashed [29] have used the Runge-Kutta method to investigate the MHD dusty nanofluid flow through the peristaltic curved channel. Saba et al. [30] have utilized NDSolve command in Mathematica to talk about the points of curved geometry and MHD on the Maxwell's nanofluid flow through peristaltic mechanism. Nadeem and Shahzadi [31] have executed the MHD nanofluid transport in a peristaltic channel having some significant curvature. Rashed and Ahmed [32] have presented the shooting scheme to achieve solutions for the nanofluid flow through the MHD curved peristaltic configuration. Ijaz et al. [33] have used Mathematica to incorporate the results of nanofluid flow with the effects of electro-MHD and curved peristaltic channel. Nadeem et al. [34] have assumed series form expressions for the Williamson nano-liquid flow through curved complaint peristaltic walls.

All the above mentioned works have been done for simple nanoparticles and none of those discussed the effects of various shapes of particles. In this study we emphasized on the effects various nanoparticles shapes which have affected the flow properties in a quite comprehensive manner. This study can be very helpful for considering a particular shape of nanoparticles to get desired benefits by nanoparticles. It is also worth mentioning that electro osmosis is not discussed for this problem in literature so this work also includes the effects of elctro-osmosis on the flow. Current model has application in targeted or smart drugging. Smart drugging is phenomena which enhance amount of drug in effected parts of the body as compare to rest of the body. As in case of case these drugs can be used to stop cancer signals which help to grow cancer cells. It is also considerable that the nanofluid pumping stream has not been discussed in literature under magnetic field and electroosmotic effects inside a curved enclosure. In the view of latest literature many authors are motivated for such flow problems to establish current study. In this article, peristaltic transport of nanofluid with different shapes of particles is considered. The effects of electrically induced magnetic field and Ohmic term are also included to enhance the worth of the study. The nanoparticles are in cylinder, platelet, brick, and blade shapes. The governing equations have been restructured by inducing

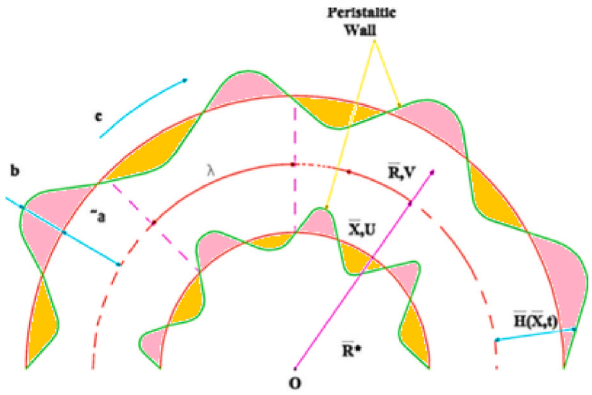

Fig. 1. Geometry of electroosmosis-modulated peristaltic transport in a two-dimensional curved channel.

new dimensionless quantities followed by a wave frame strategy. Physical properties of various shapes of nanofluid are taken into consideration while drawing figures. Physical phenomena are discussed graphically which closely relate the findings with physical scenario.

2. Quantitative formulation

2.1. Geometry of the problem

Alumina-dihydrogen monoxide non-compressible nanofluid is postulated to permeate a curved channel. The radius and the semi width curved channel is $\widetilde{R}^*$ and $\widetilde{a}$ with center at O as exhibited in Fig. 1. Moreover, the long peristaltic stream possessing the length size λ, small heights (amplitudes) $\widetilde{b}_1$ and $\widetilde{b}_2$ is assumed along the wall through speed c. In Mathematical form, the wavy walls of the geometry are represented as [35]:

$$\overline{H}(\overline{X},\overline{t}) = \pm\widetilde{a} \pm \widetilde{b}_1 \operatorname{Cos}\left[\frac{2\pi}{\lambda}(\overline{X}-c\overline{t})\right] \pm \widetilde{b}_2 \operatorname{Cos}\left[\frac{4\pi}{\lambda}(\overline{X}-c\overline{t})\right], \tag{1}$$

with constant temperature $\widetilde{T_1}$ and $\widetilde{T}_0$ at upper and lower walls, respectively such that $(\widetilde{T}_1 < \widetilde{T}_0)$.

2.2. Model description

The related governing equations for nanofluid in a curved geometry are defined as [35]:

$$\frac{\partial}{\partial\overline{R}}\{(\overline{R}+\widetilde{R}^*)\widetilde{V}\} + \widetilde{R}^*\frac{\partial\widetilde{U}}{\partial\overline{X}} = 0, \tag{2}$$

$$\begin{aligned}
&\rho_{nf}\left(\frac{\partial\widetilde{V}}{\partial\overline{t}} + \widetilde{V}\frac{\partial\widetilde{V}}{\partial\overline{R}} + \frac{\widetilde{R}^*(\widetilde{U})}{(\overline{R}+\widetilde{R}^*)}\frac{\partial\widetilde{V}}{\partial\overline{X}} - \frac{(\widetilde{U})^2}{(\overline{R}+\widetilde{R}^*)}\right) = -\frac{\partial\overline{p}}{\partial\overline{R}} \\
&+\mu_{nf}\left(\frac{1}{(\overline{R}+\widetilde{R}^*)}\frac{\partial}{\partial\overline{R}}\left((\overline{R}+\widetilde{R}^*)\frac{\partial\widetilde{V}}{\partial\overline{R}}\right) + \left(\frac{\widetilde{R}^*}{\overline{R}+\widetilde{R}^*}\right)^2\frac{\partial^2\widetilde{V}}{\partial\overline{X}^2} - \frac{\widetilde{V}}{(\overline{R}+\widetilde{R}^*)^2} - \frac{2\widetilde{R}^*}{(\overline{R}+\widetilde{R}^*)^2}\frac{\partial\widetilde{U}}{\partial\overline{X}}\right) - \frac{\overline{\rho}_e}{\rho_{nf}}\frac{\partial\Phi}{\partial R},
\end{aligned} \tag{3}$$

$$\begin{aligned}
&\rho_{nf}\left(\frac{\partial\widetilde{U}}{\partial\overline{t}} + \widetilde{V}\frac{\partial\widetilde{U}}{\partial\overline{R}} + \frac{\widetilde{R}^*\widetilde{U}}{(\overline{R}+\widetilde{R}^*)}\frac{\partial\widetilde{U}}{\partial\overline{X}} - \frac{\widetilde{U}\widetilde{V}}{(\overline{R}+\widetilde{R}^*)}\right) = -\frac{\widetilde{R}^*}{(\overline{R}+\widetilde{R}^*)}\frac{\partial\overline{p}}{\partial\overline{X}} - \frac{\overline{\rho}_e}{\rho_{nf}}\frac{\overline{R}}{\widehat{R}+R}\frac{\partial\Phi}{\partial X} + \\
&\mu_{nf}\left(\frac{1}{(\overline{R}+\widetilde{R}^*)}\frac{\partial}{\partial\overline{R}}\left((\overline{R}+\widetilde{R}^*)\frac{\partial\widetilde{U}}{\partial\overline{R}}\right) + \left(\frac{\widetilde{R}^*}{\overline{R}+\widetilde{R}^*}\right)^2\frac{\partial^2\widetilde{U}}{\partial\overline{X}^2} - \frac{\widetilde{U}}{(\overline{R}+\widetilde{R}^*)^2} - \frac{2\widetilde{R}^*}{(\overline{R}+\widetilde{R}^*)^2}\frac{\partial\widetilde{V}}{\partial\overline{X}}\right) + \\
&(\rho\beta)_{nf}g(\widetilde{T}-T_0) - \frac{\sigma_{nf}B_0^2\widetilde{U}}{\overline{R}+\widetilde{R}^*},
\end{aligned} \tag{4}$$

$$\begin{aligned}
&\left(\frac{\partial\widetilde{T}}{\partial\overline{t}} + \widetilde{V}\frac{\partial\widetilde{T}}{\partial\overline{R}} + \frac{\widetilde{R}^*\widetilde{U}}{(\overline{R}+\widetilde{R}^*)}\frac{\partial\widetilde{T}}{\partial\overline{X}}\right) = \alpha_{nf}\left(\frac{1}{(\overline{R}+\widetilde{R}^*)}\frac{\partial\widetilde{T}}{\partial\overline{R}} + \frac{\partial^2\widetilde{T}}{\partial\overline{R}^2} + \left(\frac{\widetilde{R}^*}{\overline{R}+\widetilde{R}^*}\right)^2\frac{\partial^2\widetilde{T}}{\partial\overline{X}^2}\right) \\
&-\frac{\mu_{nf}}{(\rho C_p)_{nf}}\left[\begin{array}{l} 2\left(\frac{\partial\widetilde{V}}{\partial\overline{R}}\right)^2 + \left(\frac{\widetilde{R}^*}{\overline{R}+\widetilde{R}^*}\frac{\partial\widetilde{V}}{\partial\overline{X}} - \frac{\widetilde{U}}{\overline{R}+\widetilde{R}^*}\right)\left(\frac{\partial\widetilde{U}}{\partial\overline{X}} - \frac{\widetilde{U}}{\overline{R}+\widetilde{R}^*} + \frac{\widetilde{R}^*}{\overline{R}+\widetilde{R}^*}\frac{\partial\widetilde{V}}{\partial\overline{X}}\right) + \\ \frac{\partial\widetilde{U}}{\partial\overline{R}}\left(\frac{\partial\widetilde{U}}{\partial\overline{R}} - \frac{\widetilde{U}}{\overline{R}+\widetilde{R}^*} + \frac{\widetilde{R}^*}{\overline{R}+\widetilde{R}^*}\frac{\partial\widetilde{V}}{\partial\overline{X}}\right) + 2\left(\frac{\widetilde{R}^*}{\overline{R}+\widetilde{R}^*}\frac{\partial\widetilde{U}}{\partial\overline{X}} + \frac{\widetilde{V}}{\overline{R}+\widetilde{R}^*}\right)^2 \end{array}\right] \\
&-\frac{\sigma_{nf}}{(\rho C_p)_{nf}}B_0^2\left(\frac{\widetilde{U}}{\overline{R}+\widetilde{R}^*}\right)^2.
\end{aligned} \tag{5}$$

Convert the frame having $(\overline{R},\overline{X})$ to frame having $(\overline{r},\overline{x})$ travelling with the wave speed c, and the transformations are given as

$$\overline{r} = \overline{R}, \overline{x} = \overline{X} - c\overline{t}, \widetilde{v} = \widetilde{V}, \widetilde{u} = \widetilde{U} - c. \tag{6}$$

Dimensionaless paramaters are,

$$\widetilde{x} = \frac{\overline{x}}{\lambda}, \widetilde{r} = \frac{\overline{r}}{\widetilde{a}}, v = \frac{\widetilde{v}}{c}, u = \frac{\widetilde{u}}{c}, \widetilde{p} = \frac{\widetilde{a}^2}{\lambda\mu c}p, \delta = \frac{\widetilde{a}}{\lambda}, \widetilde{k} = \frac{\widetilde{R}^*}{\widetilde{a}}, t = \frac{c\overline{t}}{\lambda}, Re = \frac{\rho ac\delta}{\mu_f}, \widetilde{\theta} = \frac{\widetilde{T}-T_1}{T_0-T_1}, \overline{E} = m^2U_{HS}\varphi, Br = \frac{\mu_f c^2}{k_f(T_0-T_1)},$$

$$Gr = \frac{\rho_f g\alpha a^2}{\mu_f c}(T_1-T_0), M = \left(\frac{\sigma_f}{\mu_f}\right)^{1/2}B_0\widetilde{a}, \tag{7}$$

under the long wavelength and creeping flow norms, equations (1)–(5) in wave frame [35] are directly given as:

$$\frac{\mu_{nf}}{\mu_f(\widetilde{r}+\widetilde{k})^2}\frac{\partial}{\partial\widetilde{r}}\left((\widetilde{r}+\widetilde{k})^2\frac{\partial u}{\partial\widetilde{r}}\right)+\frac{\mu_{nf}}{\mu_f(\widetilde{r}+\widetilde{k})^2}\frac{\partial}{\partial\widetilde{r}}\left((\widetilde{r}+\widetilde{k})^2\frac{u}{\widetilde{r}+\widetilde{k}}\right)= \frac{\widetilde{k}}{\widetilde{r}+\widetilde{k}}\frac{\partial p}{\partial\widetilde{x}}-Gr\frac{(\rho\beta)_{nf}}{\rho_f}\widetilde{\theta}-\frac{M^2}{(\widetilde{r}+\widetilde{k})^2}(u+1)-m^2U_{HS}\varphi, \tag{8}$$

$$\frac{1}{(\widetilde{r}+\widetilde{k})^2}\left((\widetilde{r}+\widetilde{k})\frac{\partial\widetilde{\theta}}{\partial\widetilde{r}}+(\widetilde{r}+\widetilde{k})^2\frac{\partial^2\widetilde{\theta}}{\partial\widetilde{r}^2}\right) +\frac{Brk_f}{k_{nf}(1-\varphi)^{2.5}}\left(\frac{\partial^2u}{\partial\widetilde{r}^2}+\frac{1}{(\widetilde{r}+\widetilde{k})^2}(1+u)^2+\frac{2}{(\widetilde{r}+\widetilde{k})^2}\frac{\partial u}{\partial\widetilde{r}}(1+u)\right) +\frac{\sigma_{nf}}{\sigma_f}\frac{M^2}{(\widetilde{r}+\widetilde{k})^2}(u+1)^2=0. \tag{9}$$

Flexural rigidity and viscous damping on the plate are described as [36,37].

$$\frac{\partial p}{\partial x}=E_1\frac{\partial^2\eta}{\partial t^2\partial x}+E_2\frac{\partial^2\eta}{\partial t\partial x}+E_3\frac{\partial^5\eta}{\partial x^5}\ \text{at}\ z=h(x,t)=\eta(x,t)+1, \tag{10}$$

and

$$\eta(x,t)=\varphi_1\ \mathrm{Cos}\ 2\pi(x-t)+\varphi_2\ \mathrm{Cos}\ 4\pi(x-t),$$

Equation (10) describe the pressure gradient in which $E_1=\frac{\overline{m}a^3c}{\lambda^3\mu}, E_2=\frac{Da^3}{\lambda^2\mu}, E_3=\frac{Ba^3}{c\lambda^5\mu}$.

The boundary conditions are defined as:

$$u(-h)=-1, u(h)=-1, \theta(-h)=1, \theta(h)=0, \tag{11}$$

2.3. Shapes of nanoparticles

The different shapes of (Al_2O_3) alumina of nanoparticles non-spherical ('Brick','Cylinder','Blade','Platelet') are described. The physical quantities of nanofluid are considered as:

$$\rho_{nf}=\chi\rho_s+(1-\chi)\rho_f, \tag{12}$$

$$\alpha_{nf}=\frac{k_{nf}}{(\rho C_p)_{nf}}, \tag{13}$$

$$(\rho Cp)_{nf}=(1-\chi)(\rho Cp)_f+\chi(\rho Cp)_s, \tag{14}$$

$$\beta_{nf}=\frac{(1-\chi)\rho_f\beta_f+\chi\rho_s\beta_s}{\rho_{nf}}. \tag{15}$$

$$\frac{\sigma_{nf}}{\sigma_f}=1+\frac{3\left(\frac{\sigma_s}{\sigma_f}-1\right)\chi}{\left(\frac{\sigma_s}{\sigma_f}+2\right)-\left(\frac{\sigma_s}{\sigma_f}-1\right)\chi} \tag{16}$$

Model for thermal conductivity of the substance is considered as [38].

$$k_{nf}/k_f=1+C_k^{Shape}+C_k^{Surface}, \tag{17}$$

Here, C_k^{Shape} is the factor of thermal conduction and $C_k^{Surface}$ is resistance the surface. Hamilton–Crosser relation modernized by Yu and Choi [39] of C_k^{Shape} and $C_k^{Surface}$ is defined as [39–40]:

$$C_k^{shape}=\left(1+\frac{m\chi X}{1-\chi_e X}\right)k_f, \tag{18}$$

Here X is defined as:

$$X=\frac{1}{3}\sum_{i=a,b,c}\frac{k_{pi}-k_f}{k_{pi}-(3/\psi-1)k_f}, \tag{19}$$

Sphericity of the particles ψ, thermal conductivity k_{pi}, depolarization factor k_{pi} defined as [40,41].

$$C_k^{Surface}=-f\cdot l_k, \tag{20}$$

Shape factor defined as f and l_k is Kapitza length

$$l_k = R_k k_f, \tag{21}$$

Viscosity of nano-fluid as defined in [39–41]

$$\mu_{nf} = \mu_f\left(1 + A_1\chi + A_2\chi^2\right), \tag{22}$$

Viscosity enhancement coefficients are A_1 *and* A_2.
For existing flow investigation skin friction (C_f) and Nusselt number (N_u) are represented by

$$C_f = -2\frac{\tau_w}{\rho_{nf}U_w^2}, \tag{23}$$

$$Nu_x = \frac{xq_w}{K_f(T_0 - T_1)}, \tag{24}$$

Where

$$\tau_w = \mu_{nf}\left(\frac{\partial u}{\partial r}\right), \tag{25}$$

$$q_w = -K_{nf}\frac{\partial T}{\partial r}, \tag{26}$$

Dimensionless form of skin friction and local Nusselt number are

$$C_f\frac{ca}{2\nu_f} = -2\frac{\rho_f\mu_{nf}}{\rho_{nf}\mu_f}\left(\frac{\partial u}{\partial r}\right), \tag{27}$$

$$Nu_x = -\frac{xKnf}{K_f}\frac{\partial\theta}{\partial r}, \tag{28}$$

Below are Tables 1 and 2 which enclosed the physical values of various nanoparticles shapes and the thermophysical representation of nanofluid, accordingly [42–51].

3. Discussion on numerical solutions and Pictorial results

The above system of boundary value problems (8-11) have been handled by a numerical approach on a mathematical software "Mathematica" through a built in command NDSolve. From received numerical data, some graphs have been presented which incorporate the whole sudy geometrically and relate the physical aspects as well. In this portion, a detailed explanation of graphic tendencies and resulting numerical assessment are described for the flow problematic modelled expending (solid-liquid) two phase invention for nanopartlicles in non-Newtonian fluid model againts countable flow representing factors like, Hartmann number M, cuevature k, drug particle C. The various profiles in the dynamics of considered nano-fluid model are assessed and graphically characterized. From figures, we can investigate the contribution of various shapes of nanoparticles on the flow characteristics. Figs. (2–4) describe the variations in velocity under the varying impact of some emerging flow parameters, while Figs. (5–7) display the impact of different factors on temperature function. From graphs, we mostly talk about the impact of parameters on unknown quantities by telling about how the curves are showing their variable behavior. For instance, our focus remains mainly on, where the curves are getting highest and lowest altitude as well what is their monotonic behavior. Moreover, the graphs also verify the results through satisfcation of boundary conditions.

3.1. Velocity profile

Now, the discrepancy in velocity for changed estimates of amplitude ratios at 0.13, 0.14 and 0.15 is described in Figs. 2 and 3. It is collected that by increase of the value φ_1 the velocity of fluid increases but opposite behaviour seen in case of φ_2. It suggests that variables magnitudes of wave retain corresponding impact on the flow attributes like velocity. If we compare the velocity of particle

Table 1
Influence of different nano-fluid particles shape results.

Property of Particles	Cylinder	Brike	Platelet	Blade
Shape				
ψ	0.62	0.81	0.52	0.36
f	0.58	0.19	2.22	3.29
l_k	1.79	1.85	1.44	1.59
A_1	13.5	1.9	37.5	14.6
A_2	904.4	471.4	612.6	123.3

Table 2
Thermo-physical values for base liquid and the nanoparticles.

Thermo-physical property	Water	Alumina (Al2O3)
Thermal conductivity (W/m·K)	0.6	40
Dynamic viscosity (kg/m·s)	0.001	–
Density (kg/m3)	997	3970
Heat capacitance (J/kg·K)	4179	765
Electrical conductivity	0.05	36.9×10^6

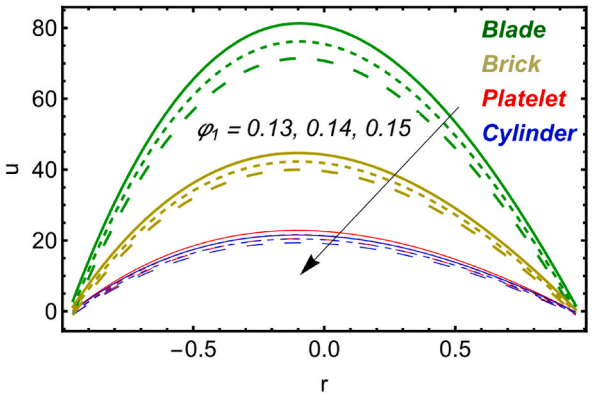

Fig. 2. Represent u curves for decreasing value for φ_1..
When $\varphi_2 = 0.14$, $M = 0.1$, $k = 5.0$, $m = 1.0$.

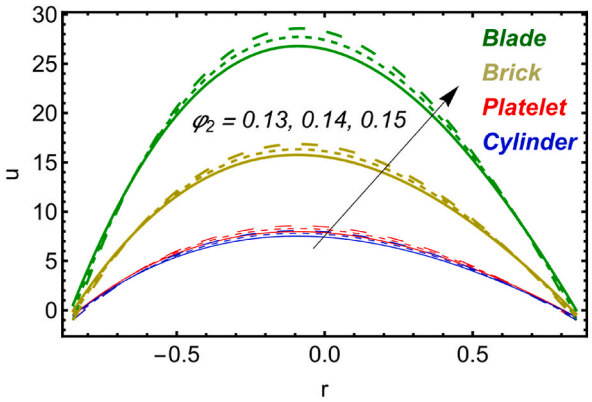

Fig. 3. Represent u curves for increasing value for φ_2..
When $\varphi_1 = 0.15$, $M = 0.1$, $k = 5.0$, $m = 1.0$.

shapes of the nanofluid, it is observed that the velocity of blade and brick shaped particle is greater the other particle shapes because of the low resistance due to smooth surface. Different values of magnetohydrodynamics 0.1, 0.2 and 0.3, the velocity variation is visible in Fig. 4. It is detected, the velocity is decreasing with rising the values of magnetohydrodynamics. Due to Lorentz force acting as a body force the fluid reduces its speed. From these figures, it is also noticeable that veloicty is a parabolic function which has maximum height at the center of the domain as compared to the boundaries of the conduit. Moreover one can easily find that the theoretical results are in well agreement with the graphic illustartions in terms of satisfaction of boundary conditions and the solution convergence as well.

3.2. Temperature profile

Figs. (5-7) are drawn for the variation on temperature with different parameters. Temperature declines in Fig. 5 with the increasing the value of curvaturer (5,10,100). So larger curvature can reduce the heat transfer rate in the flow which gives the major difference between straight channels and curved channels. The thermal performance is superlative due to the different shape of the nano-fluid particles (blade, brick, cylinder, platelet). Moreover, maximum rate of thermal exchange is measured for blades shape of nanoparticles while minimum is found for cylindrical type which means that blade shapes particles can produce a larger heat in the flow as compared

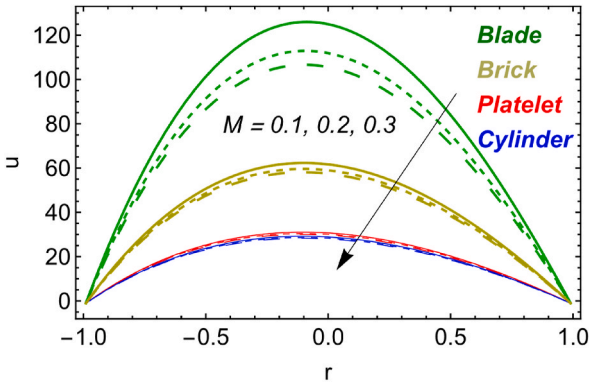

Fig. 4. Represent u curves for decreasing value for M.
When $\varphi_1 = 0.15$, $\varphi_2 = 0.14$, $k = 5.0$, $m = 1.0$.

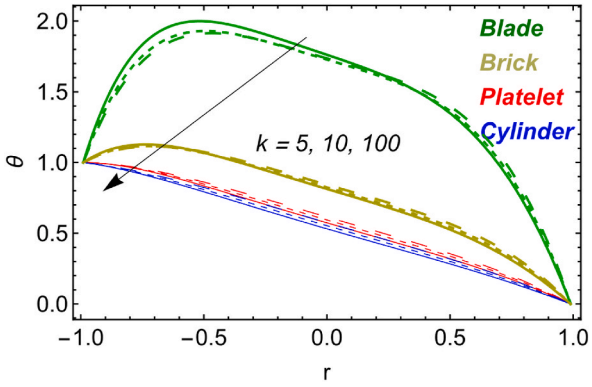

Fig. 5. Represent θ curves for decreasing value for k.
When $\varphi_1 = 0.15$, $\varphi_2 = 0.14$, $M = 0.1$, $m = 1.0$.

to other shapes taken. In Fig. 6 shows the physical effects of electo-osmosis (1.0, 3.0, 5.0) on the temperature profile. It shows that the temperature rises when we enhance the value of electric-osmosis factor so electric current can help in uplifting heat transfer in the flow and this change is prominently measured for blade shaped particles. In Fig. 7 is describes the effects of G_r on θ. With the increase of Grashof number (0.1, 0.3, 0.5) temperature displays the enhancement which is quite similar to its behavior for the variation of m.

Fig. 8 shows the skin friction parameter. It is indicated that larger the value of electo-osmosis the skin friction decelerates $-1 < r > 0$ for the different shape of the nano-fluid particles blade, brick, platelets and cylindrical. There is reverse behavior seen in the region $0 < r > 1$.

Different colors show the different shape of the nano-fluid particles such as, Green indicates blade shape particle. Yellow indicates brick shape particles. Red indicates platelets shape particles. Blue indicates cylindrical shape particles.

3.3. Streamlines' discussion

It is perceived that the lower region the flow rate is slightly lesser than that of the upper side that is why the boluses are shrinking and expanding, correspondingly. Also, socializing inner bolus grow into more elliptical in right swing of the duct as related to the left-hand side. Size of the boluses gets much bigger with increasing vale of electroosmosis like elliptic shape on the upper wall but when rising the values of both amplitudes' boluses become circular in shape as shown in Figs. 9–10. Because when the temperature is measured with higher magnitude, also compliant walls effect from lower walls of boluses to upper walls of boluses which increases the number of boluses due to compliant pumping of wall as well as peristaltically.

3.3.1. Concluding remarks

The present work having importance to deliberate the peristaltic transportation of bio-nano-fluid with different shapes of particles in a mechanical system. There are four different non-spherical particle shapes such as platelet, blade, cylinder, and brick of bio-nanoparticles are described. In complex travelling wave, water-alumina bio-nano-fluid is supposed to be movement across a curved channel. The flow is stimulated due to peristaltic movement on the compliant wall. Ohmic dissipation effects are observed during the flow of nano-fluid. The effects of electro-osmosis and mixed convection due to charged particles on the wall are examined. Summary of the present study is observed from the discussion and results of the graphs.

These outcomes are reliable with deviation of all the presented parameters.

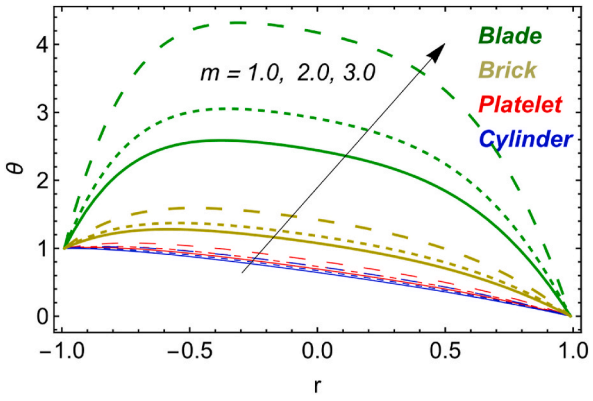

Fig. 6. Represent θ curves for increasing value for m..
When $\varphi_1 = 0.15$, $\varphi_2 = 0.14$, $k = 5.0$, $k = 5.0$.

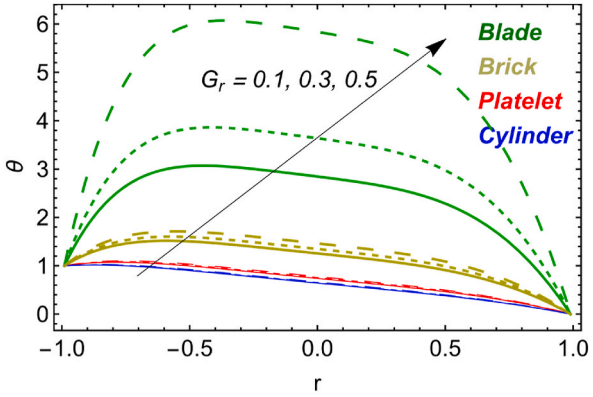

Fig. 7. Represent θ curves for increasing value for G_r.
When $\varphi_1 = 0.15$, $\varphi_2 = 0.14$, $k = 5.0$, $m = 1.0$.

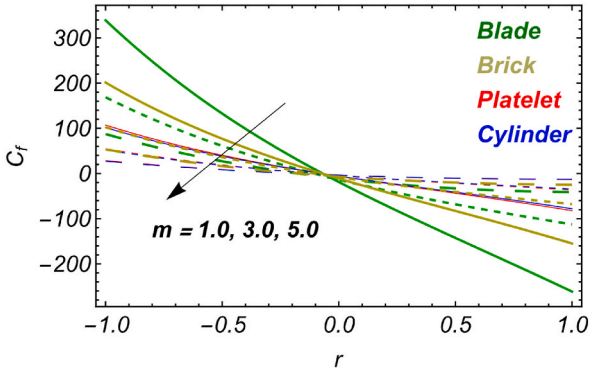

Fig. 8. Represents the Skin friction parameters.
When $\varphi_1 = 0.15$, $\varphi_2 = 0.14$, $M = 0.1$, $k = 5.0$..

- Bio-nano-fluid phase, it is availed that by increase of the value φ_1 the velocity of fluid increases but opposite behaviour seen in the flow of φ_2.
- It is found that the velocity is decreasing with rising the values of magnetohydrodynamics due to the Lorentz force.
- It is further framed that platletes shape particle much higher velocity than the cylinder shape particle by enhancing the value of elecrto-osmosis velocity of fluid are increasing.
- It is concluded that electro-kinite effects are comparable if the effects of Helmhotz-smoluchowski velocity U_{HS} are detected.
- It is declared that with increasing value of G_r the temperature of nano-fluid rises.

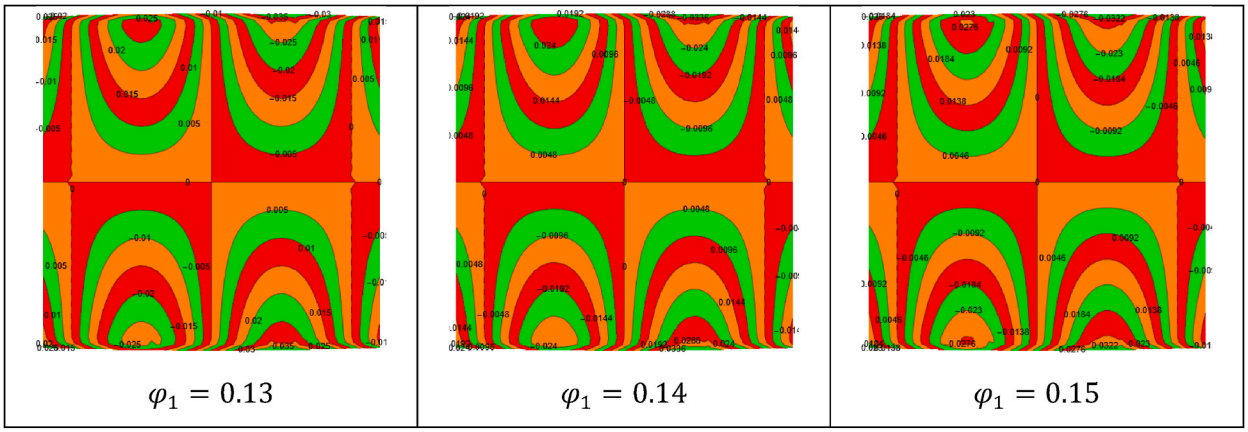

Fig. 9. Represents the Stream lines for many values of amplitude.

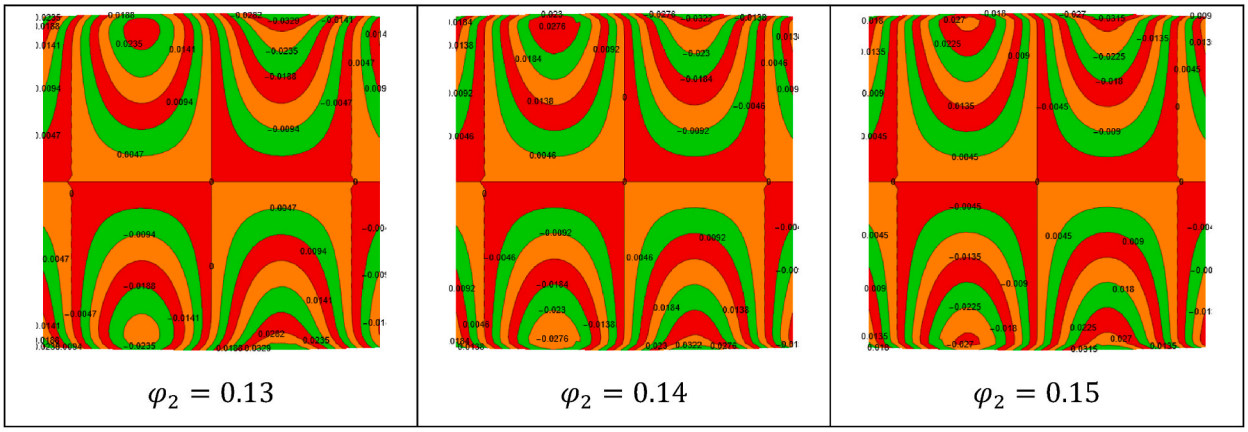

Fig. 10. Represents the Stream lines for many values of amplitude.

- In future, this study can be extended by considering some non-Newtonian fluid and some porous medium which can be a better application for fluid transport of a thicker liquid having variable viscosity inside a permeable track of flow.

Declaration of competing interest

The authors declare the following financial interests/personal relationships which may be considered as potential competing interests: Nouman Ijaz reports was provided by Punjab Group of Colleges.

Data availability

The authors do not have permission to share data.

Acknowledgments

Princess Nourah bint Abdulrahman University Researchers Supporting Project number (PNURSP2023R 371), Princess Nourah bint Abdulrahman University, Riyadh, Saudi Arabia.

References

[1] Y. Feng, C. Kleinstreuer, Thermal nanofluid property model with application to nanofluid flow in a parallel disk system—part ii: nanofluid flow between parallel disks, J. Heat Tran. 134 (5) (2012).
[2] K.V. Wong, O. De Leon, Applications of nanofluids: current and future, in: Nanotechnology and Energy, Jenny Stanford Publishing, 2017, pp. 105–132.
[3] Y. Menni, A.J. Chamkha, A. Azzi, Nanofluid transport in porous media: a review, Spec. Top Rev. Porous Media Int. J. 10 (1) (2019).
[4] N. Ali, J.A. Teixeira, A. Addali, A review on nanofluids: fabrication, stability, and thermophysical properties, J. Nanomater. (2018), 2018.
[5] C. Kleinstreuer, Z. Xu, Mathematical modeling and computer simulations of nanofluid flow with applications to cooling and lubrication, Fluid 1 (2) (2016) 16.
[6] A. Kasaeian, R. Daneshazarian, O. Mahian, L. Kolsi, A.J. Chamkha, S. Wongwises, I. Pop, Nanofluid flow and heat transfer in porous media: a review of the latest developments, Int. J. Heat Mass Tran. 107 (2017) 778–791.

[7] A. Tassaddiq, S. Khan, M. Bilal, T. Gul, S. Mukhtar, Z. Shah, E. Bonyah, Heat and mass transfer together with hybrid nanofluid flow over a rotating disk, AIP Adv. 10 (5) (2020), 055317.
[8] M. Mahdavi, M. Sharifpur, M.H. Ahmadi, J.P. Meyer, Nanofluid flow and shear layers between two parallel plates: a simulation approach, Eng. Appl. of Comput Fluid Mech. 14 (1) (2020) 1536–1545.
[9] S.K. Mondal, D. Pal, Computational analysis of bioconvective flow of nanofluid containing gyrotactic microorganisms over a nonlinear stretching sheet with variable viscosity using HAM, J. Comput. Des. Eng. 7 (2) (2020) 251–267.
[10] R. Laila, N.K.M. Dil, Nanofluid flow in a converging and diverging channel of rectangular and heated walls, Ain Shams Eng. J. 12 (4) (2021) 4023–4035.
[11] W. Alghamdi, A. Alsubie, P. Kumam, A. Saeed, T. Gul, MHD hybrid nanofluid flow comprising the medication through a blood artery, Sci. Rep. 11 (1) (2021) 1–13.
[12] T. Mehmood, M. Ramzan, F. Howari, S. Kadry, Y.M. Chu, Application of response surface methodology on the nanofluid flow over a rotating disk with autocatalytic chemical reaction and entropy generation optimization, Sci. Rep. 11 (1) (2021) 1–18.
[13] N.S. Elgazery, Nanofluids flow over a permeable unsteady stretching surface with non-uniform heat source/sink in the presence of inclined magnetic field, J. Egypt. Math. Soc. 27 (1) (2019) 1–26.
[14] K. Loganathan, N. Alessa, S. Kayikci, Heat transfer analysis of 3-D viscoelastic nanofluid flow over a convectively heated porous riga plate with Cattaneo-Christov double flux, Front. Phys. 9 (2021).
[15] T. Hayat, S. Nadeem, Induced magnetic field stagnation point flow of nanofluid past convectively heated stretching sheet with Buoyancy effects, Chin. Phys. B 25 (11) (2016), 114701.
[16] R. Ahmad, M. Mustafa, T. Hayat, A. Alsaedi, Numerical study of MHD nanofluid flow and heat transfer past a bidirectional exponentially stretching sheet, J. Magn. Magn Mater. 407 (2016) 69–74.
[17] K.V. Reddy, M.G. Reddy, O.D. Makinde, Analysis of Joule heating and chemical reaction effects in electroosmosis peristaltic transport of couple-stress and micropolar fluids, Heat Tran. 51 (6) (2022) 4992–5014.
[18] A. Ali, A. Barman, S. Das, EDL aspect in cilia-regulated bloodstream infused with hybridized nanoparticles via a microtube under a strong field of magnetic attraction, Therm. Sci. Eng. Prog. 36 (2022), 101510.
[19] N. Fatima, S. Daniel, Solution of wave equations and heat equations using HPM, in: B. Rushi Kumar, R. Sivaraj, B. Prasad, M. Nalliah, A. Reddy (Eds.), Applied Mathematics and Scientific Computing. Trends in Mathematics, Birkhäuser, Cham, 2019, https://doi.org/10.1007/978-3-030-01123-9_36.
[20] H. Vaidya, C. Rajashekhar, G. Manjunatha, K.V. Prasad, O.D. Makinde, K. Vajravelu, Heat and mass transfer analysis of MHD peristaltic flow through a complaint porous channel with variable thermal conductivity, Phys. Scripta 95 (4) (2020), 045219.
[21] N. Fatima, The study of heat conduction equation by homotopy perturbation method, SN Comput. Sci. 3 (2022) 65, https://doi.org/10.1007/s42979-021-00947-4.
[22] C. Kumawat, B.K. Sharma, K.S. Mekheimer, Mathematical analysis of two-phase blood flow through a stenosed curved artery with hematocrit and temperature dependent viscosity, Phys. Scripta 96 (12) (2021), 125277.
[23] P. Karmakar, A. Ali, S. Das, Circulation of blood loaded with trihybrid nanoparticles via electro-osmotic pumping in an eccentric endoscopic arterial canal, Int. Commun. Heat Mass Tran. 141 (2023), 106593.
[24] M.A. Abbas, Y.Q. Bai, M.M. Rashidi, M.M. Bhatti, Application of drug delivery in magnetohydrodynamics peristaltic blood flow of nanofluid in a non-uniform channel, J. Mech. Med. Biol. 16 (2016), 1650052, 04.
[25] A. Tanveer, T. Hayat, A. Alsaedi, B. Ahmad, Heat transfer analysis for peristalsis of MHD Carreau fluid in a curved channel through modified Darcy law, J. Mech. 35 (4) (2019) 527–535.
[26] A. Tanveer, T. Hayat, A. Alsaedi, Peristaltic flow of MHD Jeffery nanofluid in curved channel with convective boundary conditions: a numerical study, Neural Comput. Appl. 30 (2) (2018) 437–446.
[27] S. Noreen, M. Qasim, Z.H. Khan, MHD pressure driven flow of nanofluid in curved channel, J. Magn. Magn Mater. 393 (2015) 490–497.
[28] A. Tanveer, T. Hayat, F. Alsaadi, A. Alsaedi, Mixed convection peristaltic flow of Eyring-Powell nanofluid in a curved channel with compliant walls, Comput. Biol. Med. 82 (2017) 71–79.
[29] S.E. Ahmed, Z.Z. Rashed, MHD dusty hybrid nanofluid peristaltic flow in curved channels, Therm. Sci. 25 (2021) 4241–4255.
[30] Saba, F.M. Abbasi, S.A. Shehzad, Heat transfer analysis for EMHD peristalsis of ionic-nanofluids via curved channel with Joule dissipation and Hall effects, J. Biol. Phys. 47 (4) (2021) 455–476.
[31] S. Nadeem, I. Shahzadi, Mathematical analysis for peristaltic flow of two phase nanofluid in a curved channel, Commun. Theor. Phys. 64 (5) (2015) 547.
[32] Z.Z. Rashed, S.E. Ahmed, Peristaltic flow of dusty nanofluids in curved channels, Comput. Mater. Continua (CMC) 66 (1) (2021) 1012–1026.
[33] N. Ijaz, A. Zeeshan, S.U. Rehman, Effect of electro-osmosis and mixed convection on nano-bio-fluid with non-spherical particles in a curved channel, Mechanics & Industry 19 (1) (2018) 108.
[34] S. Nadeem, E.N. Maraj, N.S. Akbar, Investigation of peristaltic flow of Williamson nanofluid in a curved channel with compliant walls, Appl. Nanosci. 4 (5) (2014) 511–521.
[35] S. Nadeem, I. Shahzadi, Mathematical analysis for peristaltic flow of two phase nanofluid in a curved channel, Commun. Theor. Phys. 64 (5) (2015) 547.
[36] M.M. Bhatti, A. Zeeshan, R. Ellahi, N. Ijaz, Heat and mass transfer of two-phase flow with Electric double layer effects induced due to peristaltic propulsion in the presence of transverse magnetic field, J. Mol. Liq. 230 (2017) 237–246.
[37] S. Nadeem, A. Riaz, R. Ellahi, Peristaltic flow of a Jeffrey fluid in a rectangular duct having compliant walls, Chem. Ind. Chem. Eng. Q. 19 (3) (2013) 399–409.
[38] E.V. Timofeeva, J.L. Routbort, D. Singh, Particle shape effects on thermophysical properties of alumina nanofluids, J. Appl. Phys. 106 (1) (2009), 014304.
[39] W. Yu, S.U.S. Choi, The role of interfacial layers in the enhanced thermal conductivity of nanofluids: a renovated Maxwell model, J. Nanoparticle Res. 5 (1) (2003) 167–171.
[40] R. Ellahi, M. Hassan, A. Zeeshan, Shape effects of spherical and nonspherical nanoparticles in mixed convection flow over a vertical stretching permeable sheet, Mech. Adv. Mater. Struct. 24 (15) (2017) 1231–1238.
[41] A. Zeeshan, M. Hassan, R. Ellahi, M. Nawaz, Shape effect of nanosize particles in unsteady mixed convection flow of nanofluid over disk with entropy generation, Proc. IME E J. Process Mech. Eng. 231 (4) (2017) 871–879.
[42] E.V. Timofeeva, J.L. Routbort, D. Singh, Particle shape effects on thermophysical properties of alumina nanofluids, J. Appl. Phys. 106 (1) (2009), 014304.
[43] P. Goswami, J. Chakraborty, A. Bandopadhyay, S. Chakraborty, Electrokinetically modulated peristaltic transport of power-law fluids, Microvasc. Res. 103 (2016) 41–54.
[44] S. Das, P. Karmakar, A. Ali, Electrothermal blood streaming conveying hybridized nanoparticles in a non-uniform endoscopic conduit, Med. Biol. Eng. Comput. 60 (11) (2022) 3125–3151.
[45] N. Fatima, New homotopy perturbation method for solving nonlinear differential equations and Fisher type equations, in: 2017 IEEE International Conference on Power, Control, Signals and Instrumentation Engineering, ICPCSI), 2017, pp. 1669–1673, https://doi.org/10.1109/ICPCSI.2017.8391997.
[46] R. Choudhari, O.D. Makinde, F. Mebarek-Oudina, H. Vaidya, K.V. Prasad, P. Devaki, Analysis of third-grade liquid under the influence of wall slip and variable fluid properties in an inclined peristaltic channel, Heat Tran. 51 (7) (2022) 6528–6547.
[47] S.I. Abdelsalam, K.S. Mekheimer, A.Z. Zaher, Dynamism of a hybrid Casson nanofluid with laser radiation and chemical reaction through sinusoidal channels, Waves Random Complex Media (2022) 1–22.
[48] S. Das, B. Barman, R.N. Jana, O.D. Makinde, Hall and ion slip currents' impact on electromagnetic blood flow conveying hybrid nanoparticles through an endoscope with peristaltic waves, BioNanoScience 11 (3) (2021) 770–792.

[49] K.S. Mekheimer, M.A. El Kot, Suspension model for blood flow through catheterized curved artery with time-variant overlapping stenosis, Engineering Science and Technology, an International Journal 18 (3) (2015) 452–462.
[50] S. Das, B. Barman, Ramification of Hall and ion-slip currents on electro-osmosis of ionic hybrid nanofluid in a peristaltic microchannel, BioNanoScience 12 (3) (2022) 957–978.
[51] K.S. Mekheimer, R.E. Abo-Elkhair, K.K. Ali, M.G. Keshta, Entropy generation and curvature effect on peristaltic thrusting of (Cu–Al2O3) hybrid nanofluid in resilient channel: nonlinear analysis, Heat Tran. 50 (8) (2021) 7918–7948.